Occupied and unoccupied band structure of Ag(100) determined by photoemission from Ag quantum wells and bulk samples

J. J. Paggel,* T. Miller, and T.-C. Chiang

Department of Physics, University of Illinois, 1110 West Green Street, Urbana, Illinois 61801-3080
and Frederick Seitz Materials Research Laboratory, University of Illinois, 104 South Goodwin Avenue, Urbana, Illinois 61801-2902
(Received 26 August 1999)

Angle-resolved photoemission spectra taken from atomically uniform films of Ag on Fe(100) show layer-resolved quantum-well peaks. The measured peak positions as a function of film thickness permit a unique determination of the initial band dispersion via the Bohr-Sommerfeld quantization rule. This information, combined with normal-emission data taken from a single crystal Ag(100), leads to a unique determination of the final band dispersion. In this study, we employ a two-band model with four adjustable parameters for a simultaneous fit to these experimental results. The initial and final band dispersions deduced from the fit are accurate to better than 0.03 eV at any wave vector $\mathbf{k}$ within the range of measurement. The analytic formula for the band dispersions and the parameters for the best fit are given for future reference. The Fermi wave vector along [100], normalized to the Brillouin-zone size, is determined to be $\mathbf{k}_F/\mathbf{k}_{\Gamma X}=0.828\pm0.001$, which is more accurate than the de Haas–van Alphen result. The corresponding Fermi velocity is $\nu_F=1.06$ in units of the free-electron value. The combined reflection phase for the electron wave at the two boundaries is also deduced and compared with a semiempirical formula. This comparison allows us to deduce the edges of the hybridization gap in the Fe substrate.

I. INTRODUCTION

An important application of angle-resolved photoemission is band-structure determination of solids.[1] Photoemission involves an optical transition from an occupied (initial) state to an unoccupied (final) state, and the resulting spectra generally depend on both the initial and final band properties. The information is thus convoluted, and much of the historical development of the angle-resolved photoemission technique has focused on methods to untangle this information such that the initial band properties, the dispersion relation in particular, can be extracted accurately. While this is straightforward for two-dimensional systems such as layer compounds and surface states, this is a major problem for three-dimensional systems. Because the surface of a crystal breaks the translational symmetry, momentum conservation does not hold along the surface normal direction. The momentum component perpendicular to the surface, $\mathbf{k}_\perp$, of the photo-electron outside the crystal can be measured accurately, but this information is generally insufficient for a determination of $\mathbf{k}_\perp$ for the initial state inside the crystal. In contrast, the parallel component of the momentum, $\mathbf{k}_\parallel$, is conserved, and this is the only component of interest for two-dimensional systems. This "$\mathbf{k}_\perp$ problem" for three-dimensional systems has been the subject of much research, and many methods have been devised to overcome this difficulty with varying degrees of success and utility. Generally, approximations, interpolations, and/or theoretical calculations are invoked in these methods, resulting in an uncertainty of $\Delta\mathbf{k}_\perp$ typically on the order of one-tenth of the Brillouin zone size at an arbitrary point in $\mathbf{k}$ space. Another related problem is that the measured photoemission line shape is often quite broad because it is dominated by a very large final-state lifetime width.[2,3] Furthermore, the line shape can be distorted by interference from surface photoemission.[4] As a result of these complications, an energy uncertainty of $\Delta E=0.1-0.2$ eV is typical. These energy and momentum uncertainties are much too large for modern research in many-body interactions and phase-transition effects near the Fermi surface, and essentially all recent high-resolution studies in such areas have been limited to two-dimensional systems.

Loly and Pendry[5] pointed out already in 1983 that photoemission from thin films might be a way to solve the $\mathbf{k}_\perp$ problem. The basic idea is that $\mathbf{k}_\perp$ may no longer be a continuous variable as in an infinite solid. The finite thickness of the film can lead to quantization within the film, resulting in a set of discrete $\mathbf{k}_\perp$ values determined by the film thickness and boundary conditions. Photoemission should reveal a set of peaks at positions corresponding to these allowed $\mathbf{k}_\perp$ values. Although it was an interesting idea, their work went largely unnoticed because the predicted quantization effects had never been observed despite numerous photoemission studies of thin films. In retrospect, the failure for experimental observation then was most likely a consequence of extreme sample imperfections. Discrete film states, also known as quantum-well states, were observed a few years later,[6–8] and quantum-well spectroscopy has since flourished. Although the original idea of solving the $\mathbf{k}_\perp$ problem was realized and demonstrated in a few cases, this method did not offer much improvement in experimental band dispersions.[9,10] The uncertainty $\Delta\mathbf{k}_\perp$ remained quite large due to film thickness fluctuation and uncertainty. To determine $E(\mathbf{k}_\perp)$ accurately, several precisely known film thicknesses in terms of the atomic layer thickness are required. Few films made in the laboratory are uniform on an atomic scale, and even the average thickness is often uncertain by 10% or more based on standard laboratory methods of film preparation.

Recent success in preparing atomically uniform films[11,12] has finally made a precise band-structure determination based on quantum-well spectroscopy possible. The purpose of this paper is to document in detail the process in which a highly accurate band structure of Ag is derived from quantum-well measurements of atomically uniform films of Ag(100) grown on Fe(100). The accuracy is sufficiently high to challenge the Fermi wave vector determined by the venerable de Haas–van Alphen method.[13] The final band dispersion of Ag is also deduced using normal-emission data taken from a bulk Ag(100) single crystal. Both the initial and final bands are fitted simultaneously using a two-band model with four adjustable parameters, and these parameters and the analytic formula are given for future reference. The quantum well analysis also yields gap parameters for Fe(100) which have been difficult to obtain otherwise.

II. EXPERIMENTAL DETAILS

The photoemission experiment was performed using the Four-Meter Normal Incidence Monochromator at the Synchrotron Radiation Center of the University of Wisconsin, in Stoughton, Wisconsin. Photoelectrons emitted normal to the sample surface were detected with a hemispherical analyzer. The total-energy resolution of the experiment was about 50 meV. Fe whiskers were used as substrates. These were prepared by numerous cycles of Ar^+-ion sputtering at energies between 0.5 and 1.5 keV starting at room temperature and ending at 550 °C. After sputtering the sample was annealed for 5 min at 600 °C. A freshly prepared surface exhibited the very pronounced but extremely contamination-sensitive Fe(100) surface state.[14]

An effusion cell was used to deposit Ag on the substrate surface at a temperature of 100 K. The growth rate, about 0.5 ML per minute, was monitored by a quartz thickness monitor. The actual amount of deposited Ag was determined by following the evolution of quantum well peaks as a function of film thickness for layer thickness up to 20 ML (see below). The thickness monitor had been calibrated previously based on layer growth characteristics and reconstructions observed for various systems, and its nominal reading was consistent with the absolute film thickness determined by the quantum-well method to within 5%. After deposition at 100 K the film was annealed to 300 °C for 90 s and cooled back down to 100 K for the photoemission measurements. This procedure led to sharp and pronounced quantum well peaks.

If the film coverage was not an exact integer multiple of monolayers either by design or due to a 5% experimental error in deposition, two sets of quantum-well peaks derived from two thicknesses differing by 1 ML would coexist in the spectra. By regrowing submonolayer amounts of Ag on the film, and subsequently annealing the film as discussed above, it was possible to make up the difference to the next integer multiple and obtain atomically uniform films. Starting from a bare substrate, a series of absolute film thickness calibration could be made at $N = 1, 2, 3, \ldots$ as the film was built up gradually by submonolayer depositions. Such a procedure was followed in our experiment for N up to 20. This data set was sufficiently large to establish a unique functional relationship between the film thickness and quantum-well peak positions, which could be used for higher thicknesses by ex-
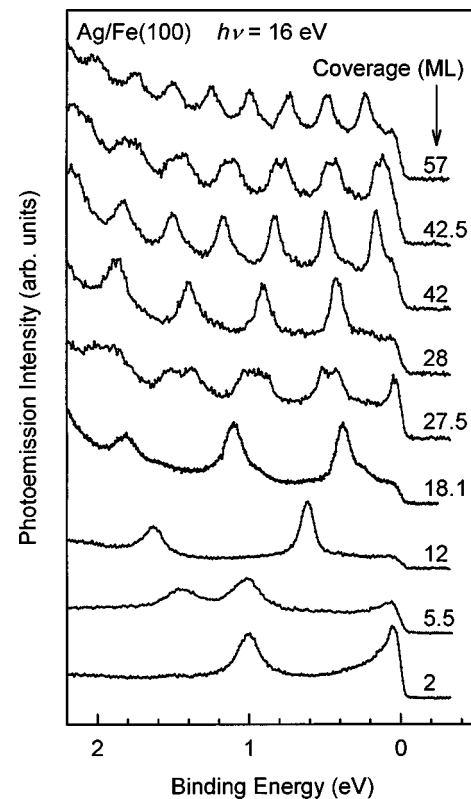

FIG. 1. A set of normal-emission spectra for Ag films on Fe(100). The coverages are indicated. All spectra are taken at a photon energy of $h\nu = 16$ eV.

trapolation. Additional layers at N greater than 20 were prepared and the peak positions were consistent with this relationship.

III. RESULTS AND DISCUSSION

A. Layer resolution and atomically uniform films

Figure 1 shows a selected set of normal-emission spectra at various Ag coverages as indicated. All spectra were taken with a photon energy of 16 eV. The bottom spectrum in Fig. 1 is taken from a 2-ML-thick Ag film, and shows a quantum-well peak at a binding energy of about 1 eV. The peak at the Fermi level is the remnant of a Fe substrate feature. The second spectrum, taken from a 5.5-ML-thick film, shows two quantum-well peaks. The one at 1.44 eV corresponds to a film thickness of 5 ML, and the other at 1.04 eV corresponds to a film thickness of 6 ML. The next spectrum is for a 12-ML coverage, and two quantum-well peaks are seen. The 18.1-ML spectrum shows three major quantum-well peaks corresponding to $N = 18$. On the lower-binding-energy side of each peak is a very small satellite peak; these satellite peaks are quantum-well peaks corresponding to $N = 19$. The intensity ratio between the satellite peak and the main peak is not the same for the three pairs because the cross sections of these quantum-well peaks are not necessarily the same, and depend on N and the photon energy used.[15]

The spectrum for 27.5-ML coverage shows two sets of peaks; one set, being at higher binding energies, corresponds to $N = 27$, and the other set corresponds to $N = 28$. The peak just below the Fermi level is for $N = 27$, and the correspond-
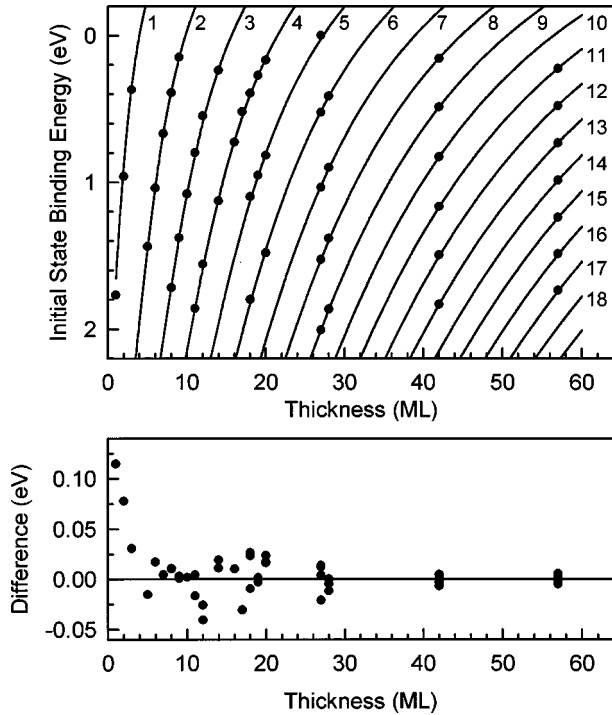
FIG. 2. The top panel is a structure plot showing the quantum-well peak binding energies as a function of film thickness. The circles are data points, and the curves are computed using parameters from a best fit. The quantum number n for each curve is shown. The bottom panel shows the difference between the best fit and experiment using an amplified vertical scale.

ing peak for $N=28$ is above the Fermi level and therefore not observed. The next spectrum was obtained by adding 0.5 ML to this 27.5-ML film to yield a 28-ML film. The set of $N=27$ peaks is now completely suppressed, and the set of $N=28$ peaks becomes twice as intense as before. This behavior illustrates the layer resolution and atomic uniformness of the films at integer coverages. A similar behavior is evident by comparing the 42- and 42.5-ML spectra. The 42-ML spectrum shows just one set of quantum-well peaks. Adding 0.5 ML to this film results in a reduction of these peaks and the appearance of a new set of peaks at lower binding energies, which correspond to $N=43$.

The spectra are analyzed by fitting to a set of Voigt peaks superimposed on a smooth background function. The Voigt function is a convolution of a Lorentzian with a Gaussian to account for lifetime broadening and instrumental effects. The resulting peak positions as a function of layer thickness are shown as circles in the structure plot presented in Fig. 2. The curves are fits based on the Bohr-Sommerfeld quantization rule and a two-band model to be presented below.

B. Bohr-Sommerfeld quantization rule

The Bohr-Sommerfeld quantization rule is given by the equation

$$2k(E)Nt + \Phi(E) = 2n\pi, \tag{1}$$

where k is the initial-state wave-vector component perpendicular to the surface, E is the binding energy, t is the monolayer thickness, Φ is the total phase shift of reflection at the

surface and the Ag-Fe interface, and n is a quantum number. Since we employ a normal-emission geometry, the wave vector is limited to the direction perpendicular to the surface ($\mathbf{k}_\parallel = 0$ and $\mathbf{k} = \mathbf{k}_\perp$). Equation (1) states that the total phase shift in a round trip perpendicular to the surface is equal to an integer (quantum number n) times 2π. Under this condition, the de Broglie wave associated with the valence electron for each n forms a standing wave or a stationary state. Photoemission from this stationary state gives rise to a peak as observed in experiment. Equation (1) is sometimes referred to as the phase accumulation model in the literature,[16–21] and its origin dates back to the beginning of quantum mechanics. Reference 12 gives a simple derivation of this equation in the context of photoemission from a film. It also shows that quantum-well states are similar to the Fabry-Pérot modes in an interferometer. Quantum well spectroscopy is essentially an interferometric measurement, and can be highly accurate if the interferometer thickness is known precisely.

C. Two-band model

It is convenient to work with a simple analytic form of the band dispersion relations with the minimum number of parameters needed to reproduce the band structure. A standard model for the Ag sp band near the Fermi level is the usual two-band model described in solid-state textbooks. Two plane-wave components and a single pseudopotential form factor are employed.[20] The wave vector $\mathbf{k}$ as a function of binding energy E (referred to the Fermi level) is given by

$$k_{i,f} = \left(\frac{2m_{i,f}}{\hbar^2}\right)^{1/2} \left\{ \frac{\hbar^2 p^2}{m_{i,f}} - V + E_{\text{vbm}} - E - \left[V^2 + 4\left(\frac{\hbar^2 p^2}{2m_{i,f}} - V \right.\right. \right.$$
$$\left.\left.\left. + E_{\text{vbm}} - E \right) \frac{\hbar^2 p^2}{2m_{i,f}} \right]^{1/2} \right\}^{1/2}, \tag{2}$$

where the wave vector $\mathbf{k}$ is measured from the X point, $p \equiv \pi/t$ is the distance between the Γ and X points in $\mathbf{k}$ space, the subscripts i and f refer to the initial and final bands, respectively, $m_{i,f}$ are effective masses associated with the initial and final bands, respectively, V is the absolute value of the pseudopotential form factor and equals one-half of the gap at the zone boundary, and E_{vbm} is the binding energy of the valence-band maximum [a negative quantity for Ag(100) since the valence-band maximum is above the Fermi level]. This model contains four adjustable parameters $m_{i,f}$, V, and E_{vbm}. The parameters V and E_{vbm} determine the positions of the band edges, and these are the only parameters used in the standard nearly free-electron model. The free-electron mass in the same model is replaced by the parameters $m_{i,f}$ in order to set the curvatures of the initial and final bands correctly. They represent higher-order corrections from multiband effects. Note that $m_{i,f}$ do not equal the inverse curvatures of the bands. There are other ways to parametrize the band structure,[20] but four parameters represent the minimum requirement.

Equation (2) can be inverted to express the binding energy E (increasing downward) in terms of $\mathbf{k}$. The formula is

$$E = E_{\text{vbm}} - V - \frac{\hbar^2 k^2}{2m_{i,f}} \pm \left(4\frac{\hbar^2 p^2}{2m_{i,f}}\frac{\hbar^2 k^2}{2m_{i,f}} + V^2 \right)^{1/2}, \tag{3}$$

where the $+$ sign and m_i should be used for the initial band, and the $-$ sign and m_f should be used for the final band.

Note that in the above equations we have chosen to measure $\mathbf{k}$ from the band edge at the X point (the distance from the zone center to the X point is π/t). One could choose instead to measure $\mathbf{k}$ from the zone center.[16–19] The different choices are really a matter of personal taste, but the quantum number n will depend on this choice. Our choice is more convenient in the present case because the observed quantum well states are all near the X point. The wave vector $\mathbf{k}$ is small near the X point, and the quantum number n is also small in accordance with Eq. (1). The $n=0$ state is closest to the top of the valence band, the $n=1$ state is the next one down, etc. A physical interpretation of the quantum number n can be made in terms of the number of antinodes of the envelope function of the probability density function in the quantum well.[22] The concept of envelope function is useful only near the Brillouin-zone boundary. With the other choice of $\mathbf{k}$, $n\cong N$ according to Eq. (1), because $\mathbf{k}\cong\pi/t$ near the X point. For a thick film such as $N=57$, the relevant quantum numbers are $n=57,56,55,\dots$ for the peaks near the X point. The state closest to the valence-band maximum has quantum number $n=N$, and the next one down has $n=N-1$, etc. When the film thickness changes by 1 ML the quantum number for the state closest to the valence-band maximum changes by one, and so do all of the other states nearby. The quantum number n is related to the number of antinodes of the probability density function itself. Each time the film thickness changes by 1 ML, an additional antinode is added within the quantum well. It is a little awkward to work with such large quantum numbers that change with film thickness, and often an offset by the layer thickness is made to simplify the coding scheme.[16] This alternate choice of $\mathbf{k}$ would be more convenient for quantum well states near the Γ point.

Most films examined in previous photoemission work were quite rough on the atomic scale, and therefore individual quantum well peaks from different discrete thicknesses in a given film are not resolved. Quantum-well peaks for such films are broad and represent the average thickness of the film. As the film coverage increases, the quantum-well peaks appear to evolve continuously rather than discretely as in the case of atomically uniform films. With our labeling scheme, the peak closest to the valence band maximum is always the $n=0$ state, etc. Each peak for a given n thus evolves smoothly, and they all converge asymptotically to the valence-band maximum as N becomes very large. With the other scheme, each smoothly evolving peak would be assigned a continuously changing average quantum number, and this would be a little cumbersome.

D. Normal-emission data from bulk Ag(100)

Figure 3 shows a set of normal-emission spectra taken from bulk Ag(100). The peak positions are determined by

$$h\nu = E_i(k) - E_f(k), \qquad (4)$$

where $h\nu$ is the photon energy, and $E_{i,f}$ are the initial and final binding energies, respectively (E_i is positive and E_f is negative). The set of spectra provides some constraints on the two-band model mentioned above. A unique solution of the band structure is, however, impossible with Eq. (4) alone. For a given $h\nu$, only the difference between the initial and
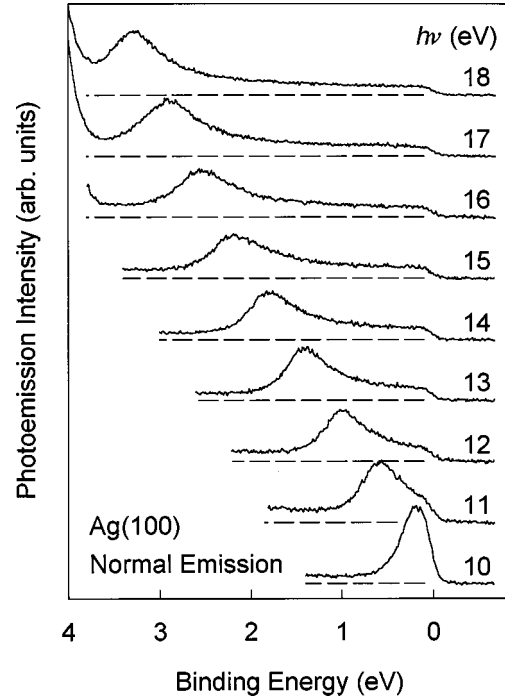

FIG. 3. A set of normal-emission spectra from Ag(100) used in our band-structure analysis.

final band energies is known, and this does not provide any information about k. For example, one could rescale k in Eq. (4) by an arbitrary factor, and the resulting equation would still be consistent with the normal emission data. The complete lack of $\mathbf{k}$ constraints is the origin of the $\mathbf{k}_\perp$ problem mentioned earlier. If the initial band structure is known, the final band structure is then uniquely determined by Eq. (4), and vice versa.

The spectra in Fig. 3 are rather broad, and the peaks are obviously asymmetric. The width is dominated by a final-state lifetime contribution. The asymmetry is due to interference from surface photoemission. A detailed analysis of this line shape was discussed in the literature,[4,23] and the resulting peak positions, E_i, are used for the band-structure analysis to be presented below.

E. Band-structure determination

Quantum-well spectra alone allow a unique determination of the initial band dispersion. In Eq. (1), both k and Φ are dependent on E, but these two unknown functions can be decoupled because of the multiplicative factor N associated with k only. It is thus important to have data for different thicknesses. If quantum well state n for thickness N happens to be at the same energy E as that of quantum well state n' for thickness N', we will have the additional phase relation

$$2kN't + \Phi = 2n'\pi, \qquad (5)$$

where k and Φ are the same as before in Eq. (1) because E is the same. Equations (1) and (5) can be solved to yield k and Φ at E in terms of the known quantities N, N', n, n', and t. Of course, it is rather seldom that quantum-well peaks from different thicknesses happen to have the same energy, but mathematical interpolation can be employed because k and

TABLE I. Parameters values for the Ag(100) band structure (m_e denotes the free-electron mass).

Parameter	Value
V	3.033 eV
E_{vbm}	−1.721 eV
m_i	$0.759 m_e$
m_f	$0.890 m_e$

Φ are continuous functions of E. In practice, a number of thicknesses are used in the experiment to determine $k(E)$ and $\Phi(E)$ via a least-squares fitting procedure. The band dispersion $E(k)$ is obtained by inverting $k(E)$.

For our fitting analysis, we use the two-band model formula discussed above for $k(E)$. The boundary phase shift $\Phi(E)$ is modeled by a third-order polynomial within the energy range of interest (between 0 and 2 eV). The final band information is provided by the normal-emission data from bulk Ag(100). Equations (1), (2), and (4) are used to fit the quantum-well data and the bulk crystal data simultaneously (with the $N = 1-3$ quantum-well data excluded; see below). In all, a total of 46 quantum-well peak positions and nine normal-emission peak positions are used in this simultaneous fit. The resulting four band structure parameters are presented in Table I. As mentioned above, the quantum-well data alone are sufficient to determine the initial band dispersion. The addition of the normal-emission data from the bulk crystal to the fitting procedure allows the final band dispersion to be determined.

The quality of the fit is excellent. The curves in Fig. 2 are predictions of the quantum well peak positions as a function of film thickness N based on the fit. Although N is an integer by definition, this calculation assumes that it is a continuous variable. These continuous curves illustrate the evolution of peak position (at large N) for each quantum number n, which is given in the figure. The differences between the curves and the data points are too small to be noticeable. The bottom panel in Fig. 2 shows the differences using an amplified vertical scale. There are no systematic deviations except for $N = 1, 2,$ and 3, and the average error amounts to ~ 20 meV. For $N = 1-3$, the deviation can be attributed to overlap of the surface and interface potentials. The screening length in a metal is quite short, and therefore the surface and interface potential steps are fairly short ranged. Nonetheless, there can be a significant overlap at very small film thicknesses, and Eq. (1), based on the assumption that the phase shifts at the two boundaries are independent and additive, is no longer valid. For this reason, the quantum well data for $N = 1-3$ are excluded from the fit as mentioned above. The same reasoning explains why this model fails at $N = 0$.[16]

The initial and final band dispersion relations deduced from the fit are plotted as solid curves in Fig. 4. The circles represent the final states reached by direct transitions from the initial band based on the normal emission data from bulk Ag(100). The positions of these circles are in excellent agreement with our fit. We have performed additional fitting analyses in which data points were added or subtracted from the fitting procedure [including removing the normal-emission data from bulk Ag(100) to yield the initial band dispersion only], and the results are consistent to within 30
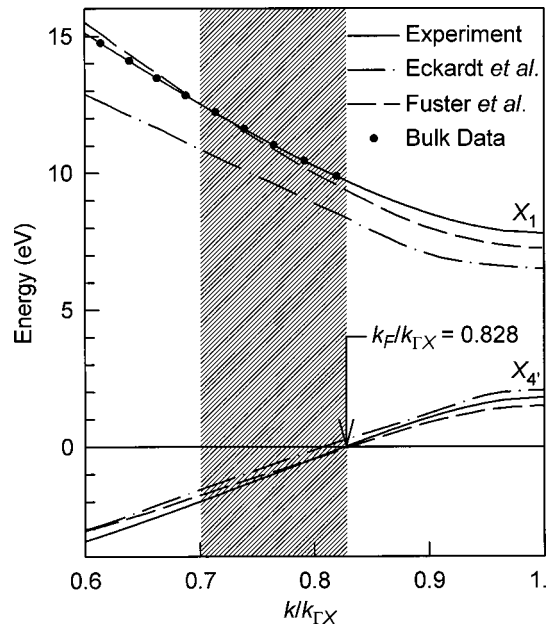

FIG. 4. Band dispersions of Ag from our best fit (solid curves) and from calculations by Refs. 24 (dash-dotted curves) and 25 (dashed curves). The circles indicate the final states based on the normal-emission spectra from bulk Ag(100). The shaded region indicates where we have data from both quantum wells and bulk single crystals. Outside this range, the dispersion curves are simply an extrapolation based on the best-fit two-band model.

meV, which is similar to the deviations seen in the bottom panel in Fig. 2. Thus, it appears that our band dispersions are accurate to this level. This statement applies only to the shaded region indicated in Fig. 4, where the quantum-well peaks are observed (within 0–2 eV below the Fermi level). The dispersions elsewhere represent an extrapolation based on the two-band model, and the uncertainty can be larger.

The dashed and dash-dotted curves in Fig. 4 indicate the results of two-band structure calculations, one in Ref. 24 and the other in Ref. 25. These calculations are chosen as representative for the large number of available results (see Ref. 25 for a discussion). The differences between various calculations are much larger than our experimental accuracy. This figure illustrates the level of accuracy of modern band-structure calculations.

F. Fermi-level crossing and band edges

An important quantity associated with the band structure is the Fermi wave vector. Our measurement yields a normalized Fermi wave vector of $\mathbf{k}_F / \mathbf{k}_{\Gamma X} = 0.828 \pm 0.001$. This differs from the de Haas–van Alphen value of 0.819.[13] This discrepancy cannot be attributed to a sample temperature difference, as we have carried out a temperature dependent measurement[26] and by extrapolation, the Fermi wave vector changes negligibly from 100 to 0 K. The de Haas–van Alphen method has been the standard method of choice for Fermi-surface measurements, but it gives only the circumference of the Fermi surface. The Fermi wave vector is deduced from a parametrization of the Fermi surface, and the accuracy of this parametrization is not fully established. It has been shown in a radio-frequency size-effect study of the Fermi surface of Au that the de Haas–van Alphen value

along [100] is 1% too small.[27] This is very similar to the 1% discrepancy (with the same sign) found for Ag in this study.

An issue of concern is the possibility of a lattice distortion in the film samples employed in our study. Ag with a fcc structure and Fe with a bcc structure have a small lattice mismatch of 0.8% in the (100) plane. For semiconductor epitaxial systems with such a small mismatch, strained growth to a critical thickness followed by unstrained growth and defect formation is typical. For metal epitaxial systems, the situation is less clear. Since metallic bonding is not directional as the covalent bonds in semiconductors, lattice relaxation is likely to occur already at the early stages of film growth. Our films are likely unstrained in view of the fairly high annealing temperature of 300 °C. Assuming the worst case that our films are fully strained by 0.8% in the interface plane, this translates into a 0.6% expansion along the surface normal direction with a Poisson ratio of 0.37. Incorporating this change in lattice constant into the analysis leaves the band-edge parameters in the fit unchanged. However, it changes the effective masses by about 1.5%, and the effect is essentially the same as a rescaling in **k**. The band structure, when plotted against the normalized wave vector $\mathbf{k}/\mathbf{k}_{\Gamma X}$, changes by less than 1 meV in the energy range of interest (0–2-eV binding energy), and the change in the normalized Fermi wave vector is negligible. This analysis suggests that lattice strain is very unlikely an explanation for the discrepancy between the de Haas–van Alphen and quantum-well results.

Another quantity of interest is the Fermi velocity (the slope of the band at the Fermi level). Our measurement yields $\nu_F = 1.06$ in units of the free-electron value. An early determination of the same quantity based on a temperature-dependent de Haas–van Alphen method yielded a value of 0.97 ± 0.03.[28] The lower band edge at the X point ($X_{4'}$ is the valence-band maximum) is 1.72 eV above the Fermi level from our determination. The is in good agreement with the two estimates given by Himpsel and Ortega[29] of 1.6 and 1.9 eV as the lower and upper bounds. The Fermi-level crossing of the direct transition peak in normal emission is at $h\nu = 9.69$ eV based on our determination, and this agrees well with the result of $h\nu = 9.6$ eV from Himpsel and Ortega.[29]

G. Boundary phase shifts and the band edges of Fe(100)

The boundary phase-shift function $\Phi(E)$ from our fit is shown in Fig. 5 as the solid curve. The phase shift at the Ag-Fe interface should change by π across the Fe hybridization gap.[16] The phase shift at the Ag surface also changes over the same energy range, but this change is much smaller. Smith *et al.*[16] derived a semiempirical formula for $\Phi(E)$ with the upper and lower edges of the Fe hybridization gap, E_u and E_l, as the only two adjustable parameters. If we take $E_u = 0$ eV and $E_l = 2$ eV, respectively, the result of the semiempirical formula, with the addition of an arbitrary vertical offset, yields the dashed curve in Fig. 5. It is in excellent agreement with our result, thus suggesting that the hybridization gap in Fe covers the range from 0 to 2 eV below the Fermi level. Our data show that quantum-well peaks become significantly weaker and broader at binding energies greater than 2 eV. Again, this is consistent with the lower band edge being at about 2 eV. Outside this gap, the Ag valence elec-
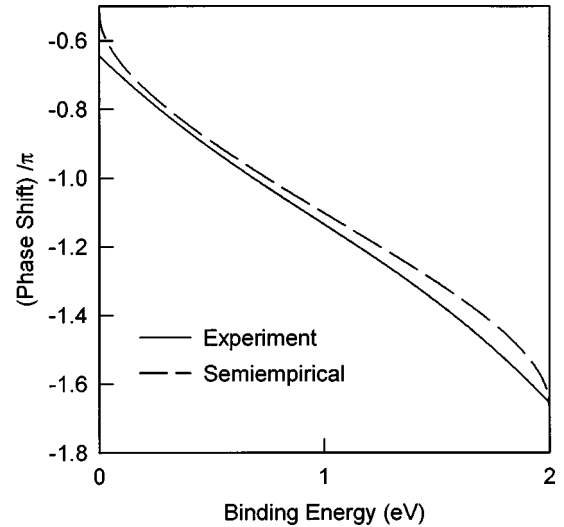

FIG. 5. Boundary phase shift as a function of binding energy. The solid curve is our experimental result, and the dashed curve is derived from a semiempirical formula as discussed in the text.

trons are no longer confined. Partial reflection at the interface could give rise to weak and broad quantum-well resonances.

Some authors have identified the hybridization gap of Fe(100) to be in between the Γ_{12} critical point and the highest point of the lowest-lying Δ_1 band.[16–19] Based on available band-structure calculations, this estimate would give $E_u = E(\Gamma_{12}) = -1.3$ eV and $E_l = E(\Delta_1^{max}) = 2.7$ eV. The gap would be about 4 eV, which is much larger than our result (2 eV). The factor of 2 discrepancy is very large, and cannot be entirely attributed to inaccuracies in band-structure calculations (up to about ± 0.5 eV). A possible explanation for this is that the hybridization between the sp and d states involves a gradual shift in orbital character, and estimating the gap boundary by visual inspection of the band dispersions is not very accurate. If we assume $E_u = E(\Gamma_{12}) = -1.3$ eV and $E_l = E(\Delta_1^{max}) = 2.7$ eV and use Smith's semiempirical formula[16] to generate the phase shift, the computed quantum-well peak positions are very much off compared to our experiment. In comparison, the peak positions derived from an *ab initio* layer-Korringa-Kohn-Rostoker calculation[19] are in much closer agreement with our experiment.

H. Spin polarization

Our experiment is not sensitive to electron spin, and therefore we do not have information about the spin polarization of the quantum-well states. Previous spin-polarized measurements at low coverages suggest that the quantum-well peaks are of the minority spin character.[17,30] As mentioned above, the Fe hybridization gap covers a range of 2 eV below the Fermi level. This is actually the minority gap, and so it is not surprising that minority quantum-well states are observed in this energy range. Available band-structure calculations show that Γ_{12} and Δ_1^{max} are at about 0.8- and 3.2-eV binding energy for the majority-spin states in Fe.[19] Assuming that the same factor of 2 correction is needed as discussed above, the majority gap should be about 1.2 eV wide. Applying the same linear mapping needed to go from the calculated Γ_{12} and Δ_1^{max} to E_u and E_l for the minority

states, we can estimate that $E_u = 1.6$ eV and $E_l = 2.8$ eV for the majority states. This range, though far below the Fermi level and relatively small, should support some majority quantum-well states. Although we have looked for them (in the form of extra peaks not explainable by the minority-spin states), we have not found any. Perhaps they are just too weak or broad (the Bohr-Sommerfeld quantization rule says nothing about the peak intensity). This lack of majority peaks is in agreement with previous work carried out at low coverages,[17,30] a quantitative explanation is not yet available.

IV. SUMMARY

Methods for bulk band-structure determination have been available for a long time, but the energy and momentum uncertainties have been too large to be of much use for modern research in electron correlation and phase-transition effects. This study documents a procedure for an accurate band-structure determination based on a combination of quantum-well spectroscopy of thin films and photoemission from bulk crystals. This procedure is carried out for Ag(100), and the resulting accuracy is better than 30 meV at a given momentum. This improvement is a direct consequence of our ability to prepare atomically uniform films. The film thicknesses, expressed in terms of the atomic layer thickness, provide a precise definition of the electron momentum. Our measurement yields a value of the Fermi wave vector $\mathbf{k}_F/\mathbf{k}_{\Gamma X} = 0.828 \pm 0.001$. This sets a new standard of accuracy, and shows that the de Haas–van Alphen value of 0.819 is off by 1%. The band structure deduced from our measurements is expressed in terms of a two-band model with four independent parameters. These parameters and the analytic formula are given for future reference. Parameters for the hybridization gap in Fe(100) are also deduced.

*Present address: Freie Universität Berlin, Institut für Experimentalphysik, 14195 Berlin, Germany.

[1] S. Hüfner, *Photoelectron Spectroscopy: Principles and Application*, 2nd ed. (Springer-Verlag, Berlin, 1996).

[2] T.-C. Chiang, J. A. Knapp, M. Aono, and D. E. Eastman, Phys. Rev. B **21**, 3513 (1980).

[3] N. V. Smith, P. Thiry, and Y. Petroff, Phys. Rev. B **47**, 15 476 (1993).

[4] T. Miller, W. E. McMahon, and T.-C. Chiang, Phys. Rev. Lett. **77**, 1167 (1996); E. D. Hansen, T. Miller, and T.-C. Chiang, *ibid.* **78**, 2807 (1997); E. D. Hansen, T. Miller, and T.-C. Chiang, Phys. Rev. B **55**, 1871 (1997).

[5] P. D. Loly and J. B. Pendry, J. Phys. C **16**, 423 (1983).

[6] A. L. Wachs, A. P. Shapiro, T. C. Hsieh, and T.-C. Chiang, Phys. Rev. B **33**, 1460 (1986).

[7] T. Miller, A. Samsavar, G. E. Franklin, and T.-C. Chiang, Phys. Rev. Lett. **61**, 1404 (1988).

[8] S.-Å. Lindgren and L. Walldén, Phys. Rev. Lett. **61**, 2894 (1988).

[9] S.-Å. Lindgren and L. Walldén, J. Phys.: Condens Matter **1**, 2151 (1989).

[10] M. A. Mueller, T. Miller, and T.-C. Chiang, Phys. Rev. B **41**, 5214 (1990).

[11] J. J. Paggel, T. Miller, and T.-C. Chiang, Phys. Rev. Lett. **81**, 5632 (1998).

[12] J. J. Paggel, T. Miller, and T.-C. Chiang, Science **283**, 1709 (1999).

[13] P. T. Coleridge and I. M. Templeton, Phys. Rev. B **25**, 7818 (1982).

[14] A. M. Turner and J. L. Erskine, Phys. Rev. B **30**, 6675 (1984).

[15] J. J. Paggel, T. Miller, and T.-C. Chiang, J. Electron Spectrosc. Relat. Phenom. **101-103**, 271 (1999).

[16] N. V. Smith, N. B. Brookes, Y. Chang, and P. D. Johnson, Phys. Rev. B **49**, 332 (1994).

[17] P. Johnson, Rep. Prog. Phys. **60**, 1217 (1997).

[18] J. E. Ortega, F. J. Himpsel, C. J. Mankey, and R. F. Willis, Phys. Rev. B **47**, 1540 (1993).

[19] S. Crampin, S. De Rossi, and F. Cicacci, Phys. Rev. B **53**, 13 817 (1996).

[20] N. V. Smith, Phys. Rev. B **32**, 3549 (1985).

[21] P. M. Echenique and J. B. Pendry, J. Phys. C **11**, 2065 (1978).

[22] W. E. McMahon, T. Miller, and T.-C. Chiang, Phys. Rev. B **54**, 10 800 (1996); W. E. McMahon, Ph.D. thesis, University of Illinois at Urbana-Champaign, 1996.

[23] E. D. Hansen, T. Miller, and T.-C. Chiang, Phys. Rev. Lett. **80**, 1766 (1998).

[24] H. Eckardt, L. Fritsche, and J. Noffke, J. Phys. F **14**, 97 (1984).

[25] G. Fuster, J. M. Tyler, N. E. Brener, J. Callaway, and D. Bagayoko, Phys. Rev. B **42**, 7322 (1990).

[26] J. J. Paggel, T. Miller, and T.-C. Chiang (unpublished).

[27] C. A. Steele and R. G. Goodrich, Phys. Rev. B **24**, 6129 (1981).

[28] M. R. Halse, Philos. Trans. R. Soc. London A **265**, 507 (1969). The Fermi velocity is related to the cyclotron mass, which can be deduced from the temperature dependence of the de Haas–van Alphen signal amplitude.

[29] F. Himpsel and J. E. Ortega, Phys. Rev. B **46**, 9719 (1992).

[30] N. B. Brookes, Y. Chang, and P. D. Johnson, Phys. Rev. Lett. **67**, 354 (1991); Phys. Rev. B **50**, 15 330 (1994).